A COMPARISON OF THE CONTINUOUS AND DISCRETE ADJOINT APPROACH TO AUTOMATIC AERODYNAMIC OPTIMIZATION

Siva K. Nadarajah[*] and Antony Jameson[†]
Department of Aeronautics and Astronautics
Stanford University
Stanford, California 94305 U.S.A.

Abstract

This paper compares the continuous and discrete adjoint-based automatic aerodynamic optimization. The objective is to study the trade-off between the complexity of the discretization of the adjoint equation for both the continuous and discrete approach, the accuracy of the resulting estimate of the gradient, and its impact on the computational cost to approach an optimum solution. First, this paper presents complete formulations and discretization of the Euler equations, the continuous adjoint equation and its counterpart the discrete adjoint equation. The differences between the continuous and discrete boundary conditions are also explored. Second, the results demonstrate two-dimensional inverse pressure design and drag minimization problems as well as the accuracy of the sensitivity derivatives obtained from continuous and discrete adjoint-based equations compared to finite-difference gradients.

Introduction

In the 1970s several attempts were made to use Computational Fluid Dynamics (CFD) as a design tool.[1–3] Since then CFD has had a significant impact. Many individuals have refocused their attention on automatic aerodynamic optimization, because of accurate numerical schemes and an exponential growth in computational speed at affordable prices. The mathematical theory for control systems governed by partial differential equations has created a framework for the formulation of inverse design and general aerodynamic problems at a reduced computational cost.[4, 5] Recently, with the help of a new generation of computers, automatic aerodynamic optimization has been revisited.[6–11]

Optimization techniques for the design of aerospace vehicles generally use gradient-based methods in which the vehicle shape is parameterized with a set of design variables. A feasible optimum shape is only achievable with an appropriate cost function. Typically such cost functions are drag coefficients, lift to drag ratios, target pressure distributions, etc. Sensitivity derivatives of the cost function with respect to the design variables are calculated by taking small steps in each and every design variable. These sensitivity derivatives are then used to get a direction of improvement and a step is taken until convergence is achieved. Each step requires a complete flow solution, and for a large number of design variables such methods are computationally costly. The mathematical theory for the control systems governed by partial differential equations, as developed, for example, by J.L. Lions,[4] decreases the cost and is more advantageous than the classical finite-difference methods.

In control theory the gradient is calculated indirectly by solving the adjoint equation. The cost of obtaining the sensitivity derivatives of the cost function with respect to each design variable from the solution of the adjoint equation is negligible in comparison with the cost of the flow calculation. Consequently, the total cost to obtain these gradients is essentially independent of the number of design variables, amounting to the cost of one flow solution and one adjoint solution, where the adjoint equation is a linear equation and thus of reduced complexity. This method was first applied to transonic flow by Jameson.[6] In the last six years automatic aerodynamic design of complete aircraft configurations has been successful, yielding optimized solutions of wing and wing-body configurations.[12–14, 16]

The continuous adjoint approach theory was developed by combining the variation of the cost func-

[*]Graduate Student, Student Member AIAA
[†]Thomas V. Jones Professor of Engineering, Stanford University, AIAA Fellow

American Institute of Aeronautics and Astronautics

tion and field equations with respect to the flow-field variables and design variables through the use of Lagrange multipliers also called costate or adjoint variables. Collecting the terms associated with the variation of the flow-field variables produces the adjoint equation and its boundary condition. The terms associated with the variation of the design variable produce the gradient. The field equations and the adjoint equation with its boundary condition must be discretized to obtain numerical solutions. As the mesh is refined, the continuous adjoint yields the exact gradient.

The discrete adjoint approach means applying the control theory directly to the set of discrete field equations. The discrete adjoint equation is derived by collecting together all the terms multiplied by the variation $\delta w_{i,j}$ of the discrete flow variable. If the discrete adjoint equation is solved exactly, then the resulting solution for the Lagrange multiplier produces an exact gradient of the inexact cost function and the derivatives are consistent with finite difference gradients independent of the mesh size.

A subject of on-going research is the trade-off between the complexity of the adjoint discretization, the accuracy of the resulting estimate of the gradient, and its impact on the computational cost to approach an optimum solution. Shubin and Frank[11] presented a comparison between the continuous and discrete adjoint for quasi-one-dimensional flow. A variation of the discrete field equations proved to be complex for higher order schemes. Due to this limitation of the discrete adjoint approach, early implementation of the discretization of the adjoint equation was only consistent with a first order accurate flow equation. Beux and Dervieux[15] used a first order upwind scheme with Van Leer flux vector splitting on a two-dimensional unstructured grid.

Burgreen and Baysal[16] carried a second order implementation of the discrete adjoint on three-dimensional shape optimization of wings for structured grids. For second order accuracy on unstructured grids, Elliot and Peraire[17] solved the Euler equations by a multistage Runge-Kutta scheme with Roe decomposition for the dissipative fluxes on two and three-dimensional unstructured grids. They performed optimization on inverse pressure designs of multielement airfoils and wing-body configurations in transonic flow. Anderson and Venkatakrishnan[18] computed inviscid and viscous optimization on unstructured grids using both the continuous and discrete adjoint. Iollo, Salas, and Ta'saan[19] investigated shape optimization on one and two-dimensional flows using the continuous adjoint ap-

proach. Ta'saan, Kuruvila, and Salas[20] used a one-shot approach with the continuous adjoint formulations. Kim, Alonso, and Jameson[21] conducted an extensive gradient accuracy study of the Euler and Navier-Stokes equations which concluded that gradients from the continuous adjoint method were in close agreement with those computed by finite difference methods, and less dependent on the level of convergence of the flow solver.

Objectives

The objectives of this work are:

1. Review the formulation and development of the compressible adjoint equations for both the continuous and discrete approach.

2. Investigate the differences in the implementation of boundary conditions for each method.

3. Compare the gradients of the two methods to finite difference gradients for inverse pressure design and drag minimization.

4. Compare the convergence between the continuous and discrete adjoint.

5. Study the differences in calculating the exact gradient of the inexact cost function (discrete adjoint) or the inexact gradient of the exact cost function (continuous).

The Design Problem as a Control Problem

A simple approach to optimization is to represent the geometry through a set of design parameters, which may, for example, be the weights α_i applied to a set of shape functions $b_i(x)$ so that the shape is represented as

$$f(x) = \sum \alpha_m b_m(x).$$

Next, a cost function I which is a function of the weight parameters α_m is chosen. Such a cost function can be the difference between the current and target pressure distribution for inverse design problems, drag coefficient for drag minimization problems, or lift to drag ratio. The sensitivities $\frac{\partial I}{\partial \alpha_m}$ may now be estimated by making a small variation $\delta \alpha_m$ in each design parameter in turn and recalculating the flow to obtain the change in I. Then, using a finite difference formula,

$$\frac{\partial I}{\partial \alpha_m} \approx \frac{I(\alpha_m + \delta \alpha_m) - I(\alpha_m)}{\delta \alpha_m}.$$

The gradient vector $\frac{\partial I}{\partial \alpha}$ may now be used to determine a direction of improvement. The simplest procedure uses the method of steepest descent and takes a step in the negative gradient direction by setting

$$\alpha^{n+1} = \alpha^n - \lambda \frac{\partial I}{\partial \alpha},$$

so that to first order

$$I + \delta I = I + \frac{\partial I^T}{\partial \alpha} \delta \alpha = I - \lambda \frac{\partial I^T}{\partial \alpha} \frac{\partial I}{\partial \alpha}.$$

The main disadvantageous of the finite difference method are first that $N + 1$ flow calculations are needed to calculate the sensitivities of N design variables, and second that the accuracy is sensitive to the step size $\delta \alpha_m$.

These difficulties are circumvented by the control theory approach which may be outlined in abstract form as follows. For flow around an airfoil, the aerodynamic properties that define the cost function are functions of the flow-field variables, w, and the physical location of the boundary, which may be represented by the function $\mathcal{F}$, say. Then

$$I = I\left(w, \mathcal{F}\right),$$

and a change in $\mathcal{F}$ results in a change

$$\delta I = \frac{\partial I^T}{\partial w} \delta w + \frac{\partial I^T}{\partial \mathcal{F}} \delta \mathcal{F}, \qquad (1)$$

in the cost function. Using control theory the governing equations of the flow-field are now introduced as a constraint in such a way that the final expression for the gradient does not require reevaluation of the flow-field. In order to achieve this δw must be eliminated from (1). Suppose that the governing equation R which expresses the dependence of w and $\mathcal{F}$ within the flow-field domain D can be written as

$$R\left(w, \mathcal{F}\right) = 0. \qquad (2)$$

Then δw is determined from the equation

$$\delta R = \left[\frac{\partial R}{\partial w}\right] \delta w + \left[\frac{\partial R}{\partial \mathcal{F}}\right] \delta \mathcal{F} = 0. \qquad (3)$$

Next, introducing a Lagrange Multiplier ψ, we have

$$\delta I = \frac{\partial I^T}{\partial w} \delta w + \frac{\partial I^T}{\partial \mathcal{F}} \delta \mathcal{F} - \psi^T \left(\left[\frac{\partial R}{\partial w}\right] \delta w + \left[\frac{\partial R}{\partial \mathcal{F}}\right] \delta \mathcal{F}\right)$$

$$= \left\{\frac{\partial I^T}{\partial w} - \psi^T \left[\frac{\partial R}{\partial w}\right]\right\} \delta w + \left\{\frac{\partial I^T}{\partial \mathcal{F}} - \psi^T \left[\frac{\partial R}{\partial \mathcal{F}}\right]\right\} \delta \mathcal{F}.$$

Choosing ψ to satisfy the adjoint equation

$$\left[\frac{\partial R}{\partial w}\right]^T \psi = \frac{\partial I}{\partial w} \qquad (4)$$

the first term is eliminated, and we find that

$$\delta I = \mathcal{G} \delta \mathcal{F}, \qquad (5)$$

where

$$\mathcal{G} = \frac{\partial I^T}{\partial \mathcal{F}} - \psi^T \left[\frac{\partial R}{\partial \mathcal{F}}\right].$$

Euler Equations

In order to allow for geometric shape changes it is convenient to use a body fitted coordinate system, so that the computational domain is fixed. This requires the formulation of the Euler equations in the transformed coordinate system. The Cartesian coordinates and velocity components are denoted by x_1, x_2, and u_1, u_2. Einstein notation simplifies the presentation of the equations, where summation over $k = 1$ to 2 is implied by a repeated index k. Then the two-dimensional compressible Euler equations may be written as

$$\frac{\partial w}{\partial t} + \frac{\partial f_k}{\partial x_k} = 0 \quad \text{in } D, \qquad (6)$$

where

$$w = \left\{\begin{array}{c} \rho \\ \rho u_1 \\ \rho u_2 \\ \rho E \end{array}\right\}, \quad f_k = \left\{\begin{array}{c} \rho u_k \\ \rho u_k u_1 + p \delta_{k1} \\ \rho u_k u_2 + p \delta_{k2} \\ \rho u_k H \end{array}\right\} \qquad (7)$$

and δ_{kl} is the Kronecker delta function. Also,

$$p = (\gamma - 1) \rho \left\{E - \frac{1}{2}\left(u_k^2\right)\right\}, \qquad (8)$$

and

$$\rho H = \rho E + p \qquad (9)$$

where γ is the ratio of the specific heats.

Consider a transformation to coordinates ξ_1, ξ_2, where

$$K_{kl} = \left[\frac{\partial x_k}{\partial \xi_l}\right], \quad J = \det\left(K\right), \quad K_{kl}^{-1} = \left[\frac{\partial \xi_k}{\partial x_l}\right],$$

and

$$S = JK^{-1}.$$

The elements of S are the coefficients of K, and in a finite volume discretization they are just the face

American Institute of Aeronautics and Astronautics

areas of the computational cells projected in the x_1 and x_2 directions. Also introduce scaled contravariant velocity components as

$$U_k = S_{kl}u_l.$$

The Euler equations can now be written as

$$\frac{\partial W}{\partial t} + \frac{\partial F_k}{\partial \xi_k} = 0 \quad \text{in } D, \tag{10}$$

where

$$W = Jw,$$

and

$$F_k = S_{kl}f_l = \begin{bmatrix} \rho U_k \\ \rho U_k u_1 + S_{l1}p \\ \rho U_k u_2 + S_{l2}p \\ \rho U_k H \end{bmatrix}. \tag{11}$$

Assume now that the new computational coordinate system conforms to the airfoil in such a way that the airfoil surface B_W is represented by $\xi_2 = 0$. Then the flow is determined as the steady state solution of equation (10) subject to the flow tangency condition

$$U_2 = 0 \quad \text{on } B_W. \tag{12}$$

At the far field boundary B_F, conditions are specified for incoming waves, as in the two-dimensional case, while outgoing waves are determined by the solution.

When equation (10) is formulated for each computational cell, a system of first-order ordinary differential equations is obtained. To eliminate odd-even decoupling of the solution and overshoots before and after shock waves, the conservative flux is added to a diffusion flux. The artificial dissipation scheme used in this research is a blended first and third order flux, first introduced by Jameson, Schmidt, and Turkel.[22] The artificial dissipation scheme is defined as,

$$D_{i+\frac{1}{2},j} = \epsilon^2_{i+\frac{1}{2},j}(w_{i+1,j} - w_{i,j})$$
$$- \epsilon^4_{i+\frac{1}{2},j}(w_{i+2,j} - 3w_{i+1,j} + 3w_{i,j} - w_{i-1,j}). \tag{13}$$

The first term in equation (13) is a first order scalar diffusion term, where $\epsilon^2_{i+\frac{1}{2},j}$ is scaled by the normalized second difference of the pressure and serves to damp oscillations around shock waves. $\epsilon^4_{i+\frac{1}{2},j}$ is the coefficient for the third derivative of the artificial dissipation flux. The coefficient is scaled such that it is zero at regions of large gradients, such as shock waves and eliminates odd-even decoupling elsewhere.

Design using the Euler Equations

This section illustrates application of control theory to aerodynamic design problems for the case of two-dimensional airfoil design using the compressible Euler equations as the mathematical model.

Continuous Adjoint

The weak form of the Euler equations for steady flow is

$$\int_{\mathcal{D}} \frac{\partial \phi^T}{\partial \xi_k} F_k d\mathcal{D} = \int_{\mathcal{B}} n_k \phi^T F_k d\mathcal{B}, \tag{14}$$

where the test vector ϕ is an arbitrary differentiable function and n_k is the outward normal at the boundary. If a differentiable solution w is obtained to this equation, then it can be integrated by parts to give

$$\int_{\mathcal{D}} \phi^T \frac{\partial F_k}{\partial \xi_k} d\mathcal{D} = 0.$$

Since this is true for any ϕ the differential form can be recovered. If the solution is discontinuous, then (14) may be integrated by parts separately on either side of the discontinuity to recover the shock jump conditions.

Suppose now that we desire to control the surface pressure by varying the wing shape. For this purpose, it is convenient to retain a fixed computational domain. Variations in the shape then result in corresponding variations in the mapping derivatives defined by K. Introduce the cost function

$$I = \frac{1}{2} \int_{B_W} (p - p_d)^2 \, ds,$$

where p_d is the desired pressure. The design problem is now treated as a control problem where the control function is the wing shape, which is chosen to minimize I subject to the constraints defined by the flow equations (10-11). A variation in the shape causes a variation δp in the pressure and consequently a variation in the cost function

$$\delta I = \int_{B_W} (p - p_d)\,\delta p \, ds + \frac{1}{2} \int_{B_W} (p - p_d)^2 \, \delta ds. \tag{15}$$

Since p depends on w through the equation of state (8–9), the variation δp is determined from the variation δw. Define the Jacobian matrices

$$A_k = \frac{\partial f_k}{\partial w}, \quad C_k = S_{kl}A_l. \tag{16}$$

4

The weak form of the equation for δw in the steady state becomes

$$\int_{\mathcal{D}} \frac{\partial \phi^T}{\partial \xi_k} \delta F_k d\mathcal{D} = \int_{\mathcal{B}} (n_k \phi^T \delta F_k) d\mathcal{B},$$

where

$$\delta F_k = C_k \delta w + \delta S_{kl} f_l,$$

which should hold for any differentiable test function ϕ. This equation may be added to the variation in the cost function, which may now be written as

$$
\begin{aligned}
\delta I \;\; = & \int_{B_W} (p - p_d)\, \delta p \;\, ds + \frac{1}{2} \int_{B_W} (p - p_d)^2 \; \delta ds \\
& - \int_{\mathcal{D}} \frac{\partial \psi^T}{\partial \xi_k} \delta F_k d\mathcal{D} + \int_{\mathcal{B}} (n_k \psi^T \delta F_k) d\mathcal{B} \qquad (17)
\end{aligned}
$$

On the wing surface B_W, $n_1 = 0$. Thus, it follows from equation (12) that

$$
\delta F_2 =
\begin{bmatrix}
0 \\
S_{21}\delta p \\
S_{22}\delta p \\
0
\end{bmatrix}
+
\begin{bmatrix}
0 \\
\delta S_{21} p \\
\delta S_{22} p \\
0
\end{bmatrix}. \qquad (18)
$$

Since the weak equation for δw should hold for an arbitrary choice of the test vector ϕ, we are free to choose ϕ to simplify the resulting expressions. Therefore we set $\phi = \psi$, where the costate vector ψ is the solution of the adjoint equation

$$\frac{\partial \psi}{\partial t} - C_k^T \frac{\partial \psi}{\partial \xi_k} = 0 \;\; \text{in } D. \qquad (19)$$

At the outer boundary incoming characteristics for ψ correspond to outgoing characteristics for δw. Consequently we can choose boundary conditions for ψ such that

$$n_k \psi^T C_k \delta w = 0.$$

If the coordinate transformation is such that δS is negligible in the far field, then the only remaining boundary term is

$$- \int_{B_W} \psi^T \delta F_2 \; d\xi_1.$$

Thus, by letting ψ satisfy the boundary condition,

$$\psi_j n_j = p - p_d \;\; \text{on } B_W, \qquad (20)$$

where n_j are the components of the surface normal,

$$n_j = \frac{S_{2j}}{\sqrt{S_{2j}S_{2j}}}$$

we find finally that

$$
\begin{aligned}
\delta I \;\; = & \frac{1}{2} \int_{B_W} (p - p_d)^2 \, \delta ds \\
& - \int_{\mathcal{D}} \frac{\partial \psi^T}{\partial \xi_k} \delta S_{kl} f_l d\mathcal{D} \\
& - \int_{B_W} (\delta S_{21}\psi_2 + \delta S_{22}\psi_3) \, p \, d\xi_1. \qquad (21)
\end{aligned}
$$

Numerical Discretization

The continuous adjoint equation is linear and consequently it could be solved by direct numerical inversion. The cost of the associated matrix inversion can become prohibitive as the number of mesh cells are increased. Instead, since the equations are similar to that of the Euler equations, the same iterative method is used to solve the continuous adjoint equation. In this research, a five stage Runge-Kutta scheme with three evaluations of the artificial dissipation scheme is used. We employ the blended first and third order scalar diffusion scheme used for the Euler equations here as well. The following is a second order discretization of the continuous adjoint equation,

$$
\begin{aligned}
V \frac{\partial \psi_{i,j}}{\partial t} = & \left(\Delta y_\eta \left[\frac{\partial f}{\partial w} \right]^T - \Delta x_\eta \left[\frac{\partial g}{\partial w} \right]^T \right)_{i,j} \left(\frac{\psi_{i+1,j}}{2} \right) \\
& - \left(\Delta y_\eta \left[\frac{\partial f}{\partial w} \right]^T - \Delta x_\eta \left[\frac{\partial g}{\partial w} \right]^T \right)_{i,j} \left(\frac{\psi_{i-1,j}}{2} \right) \\
& + \left(-\Delta y_\xi \left[\frac{\partial f}{\partial w} \right]^T + \Delta x_\xi \left[\frac{\partial g}{\partial w} \right]^T \right)_{i,j} \left(\frac{\psi_{i,j+1}}{2} \right) \\
& - \left(-\Delta y_\xi \left[\frac{\partial f}{\partial w} \right]^T + \Delta x_\xi \left[\frac{\partial g}{\partial w} \right]^T \right)_{i,j} \left(\frac{\psi_{i,j-1}}{2} \right) \\
& + d_{i+\frac{1}{2},j} - d_{i-\frac{1}{2},j} + d_{i,j+\frac{1}{2}} - d_{i,j-\frac{1}{2}}
\end{aligned}
$$
$$\qquad (22)$$

where, V is the cell area and $d_{i+\frac{1}{2},j}$ has the same form as equation (13).

In the case of the continuous adjoint boundary condition, equation (20) dictates values for the normal adjoint velocities. The choice for ψ_1, ψ_4, and the tangential adjoint velocity are arbitrary, therefore assigning a zero value for these variables does

not violate equation (20). This results, however, in a poor convergence for the adjoint equation since it is an over-specification of the adjoint boundary condition. A satisfactory boundary condition may be formulated as follows:

$$
\begin{aligned}
\psi_{1_{i,1}} &= \psi_{1_{i,2}} \\
\psi_{2_{i,1}} &= \psi_{2_{i,2}} + 2n_2 \left((p - p_d) - n_2 \psi_{2_{i,2}} + n_1 \psi_{3_{i,2}} \right) \\
\psi_{3_{i,1}} &= \psi_{3_{i,2}} - 2n_1 \left((p - p_d) - n_2 \psi_{2_{i,2}} + n_1 \psi_{3_{i,2}} \right) \\
\psi_{4_{i,1}} &= \psi_{4_{i,2}}
\end{aligned}
\tag{23}
$$

where,

$$
n_i = \frac{S_{2i}}{\sqrt{S_{2j} S_{2j}}}
$$

The subscript $i, 1$ and $i, 2$ in the above equations denote cells below and above the wall. Here, the first and fourth costate variables below the wall are set equal to the corresponding values above the wall and the tangential adjoint velocities above and below the wall are equated.

Drag Minimization

If the drag is to be minimized, then the cost function is the drag coefficient,

$$
\begin{aligned}
I &= C_d \\
&= \left(\frac{1}{c} \int_{B_W} C_p \frac{\partial y}{\partial \xi} d\xi \right) \cos \alpha \\
&+ \left(\frac{1}{c} \int_{B_W} -C_p \frac{\partial x}{\partial \xi} d\xi \right) \sin \alpha
\end{aligned}
$$

A variation in the shape causes a variation ∂p in the pressure and consequently a variation in the cost function,

$$
\begin{aligned}
\delta I &= \frac{1}{c} \int_{B_W} C_p \left(\frac{\partial y}{\partial \xi} \cos \alpha - \frac{\partial x}{\partial \xi} \sin \alpha \right) \partial p \, d\xi \\
&+ \frac{1}{c} \int_{B_W} C_p \left(\delta \left(\frac{\partial y}{\partial \xi} \right) \cos \alpha - \delta \left(\frac{\partial x}{\partial \xi} \right) \sin \alpha \right) d\xi
\end{aligned}
\tag{24}
$$

As in the inverse design case, the first term is a function of the state vector, and therefore is incorporated into the boundary condition, where the integrand replaces the pressure difference term in equation (23). The second term is added on to the gradient term.

Discrete Adjoint

The discrete adjoint equation is obtained by applying the control theory directly to the set of discrete field equations. The resulting equation depends on the type of scheme used to solve the flow equations. This paper uses, a cell centered multigrid scheme with upwind biased blended first and third order fluxes as the artificial dissipation scheme. A full discretization of the equation would involve discretizing every term that is a function of the state vector.

$$
\delta I = \delta I_c + \sum_{i=2}^{nx} \sum_{j=2}^{ny} \psi_{i,j}^T \delta \left(R(w)_{i,j} + D(w)_{i,j} \right)
\tag{25}
$$

where δI_c is the discrete cost function, $R(w)$ is the field equation, and $D(w)$ is the artificial dissipation term.

Terms multiplied by the variation $\delta w_{i,j}$ of the discrete flow variables are collected and the following is the resulting discrete adjoint equation,

$$
\begin{aligned}
V \frac{\partial \psi_{i,j}}{\partial t} &= \\
&\left(\Delta y_{\eta_{i+\frac{1}{2},j}} \left[\frac{\partial f}{\partial w} \right]_{i,j}^T - \Delta x_{\eta_{i+\frac{1}{2},j}} \left[\frac{\partial g}{\partial w} \right]_{i,j}^T \right) \frac{\psi_{i+1,j}}{2} \\
&- \left(\Delta y_{\eta_{i-\frac{1}{2},j}} \left[\frac{\partial f}{\partial w} \right]_{i,j}^T - \Delta x_{\eta_{i-\frac{1}{2},j}} \left[\frac{\partial g}{\partial w} \right]_{i,j}^T \right) \frac{\psi_{i-1,j}}{2} \\
&+ \left(\Delta x_{\xi_{i,j+\frac{1}{2}}} \left[\frac{\partial g}{\partial w} \right]_{i,j}^T - \Delta y_{\xi_{i,j+\frac{1}{2}}} \left[\frac{\partial f}{\partial w} \right]_{i,j}^T \right) \frac{\psi_{i,j+1}}{2} \\
&- \left(\Delta x_{\xi_{i,j-\frac{1}{2}}} \left[\frac{\partial g}{\partial w} \right]_{i,j}^T - \Delta y_{\xi_{i,j-\frac{1}{2}}} \left[\frac{\partial f}{\partial w} \right]_{i,j}^T \right) \frac{\psi_{i,j-1}}{2} \\
&- \left(\Delta y_{\eta_{i+\frac{1}{2},j}} \left[\frac{\partial f}{\partial w} \right]_{i,j}^T - \Delta x_{\eta_{i+\frac{1}{2},j}} \left[\frac{\partial g}{\partial w} \right]_{i,j}^T \right) \frac{\psi_{i,j}}{2} \\
&+ \left(\Delta y_{\eta_{i-\frac{1}{2},j}} \left[\frac{\partial f}{\partial w} \right]_{i,j}^T - \Delta x_{\eta_{i-\frac{1}{2},j}} \left[\frac{\partial g}{\partial w} \right]_{i,j}^T \right) \frac{\psi_{i,j}}{2} \\
&- \left(\Delta x_{\xi_{i,j+\frac{1}{2}}} \left[\frac{\partial g}{\partial w} \right]_{i,j}^T - \Delta y_{\xi_{i,j+\frac{1}{2}}} \left[\frac{\partial f}{\partial w} \right]_{i,j}^T \right) \frac{\psi_{i,j}}{2} \\
&+ \left(\Delta x_{\xi_{i,j-\frac{1}{2}}} \left[\frac{\partial g}{\partial w} \right]_{i,j}^T - \Delta y_{\xi_{i,j-\frac{1}{2}}} \left[\frac{\partial f}{\partial w} \right]_{i,j}^T \right) \frac{\psi_{i,j}}{2} \\
&+ \delta d_{i+\frac{1}{2},j} - \delta d_{i-\frac{1}{2},j} + \delta d_{i,j+\frac{1}{2}} - \delta d_{i,j-\frac{1}{2}}.
\end{aligned}
\tag{26}
$$

6

where,

$$\delta d_{i+\frac{1}{2},j} = \epsilon^2_{i+\frac{1}{2},j}(\psi_{i+1,j} - \psi_{i,j}) - \epsilon^4_{i+\frac{3}{2},j}\psi_{i+2,j}$$
$$+3\epsilon^4_{i+\frac{1}{2},j}(\psi_{i+1,j} - \psi_{i,j}) + \epsilon^4_{i-\frac{3}{2},j}\psi_{i-1,j}$$

$$(27)$$

is the discrete adjoint artificial dissipation term and V is the cell area. The dissipation coefficients ϵ^2 and ϵ^4 are functions of the flow variables, but to reduce complexity they are treated as constants. The effect of this partial discretization of the artificial dissipation term is explored in the Results section.

In the case of an inverse design, δI_c is the discrete form of equation (15). The $\delta w_{i,2}$ term is added to the corresponding term from equation (26), and the metric variation term is added to the gradient term. In contrast to the continuous adjoint, where the boundary condition appears as an update to the costate variables in the cell below the wall, the discrete boundary condition appears as a source term in the adjoint fluxes. At cell $i, 2$ the adjoint equation is as follows,

$$V\frac{\partial\psi_{i,2}}{\partial t} =$$
$$\frac{1}{2}\left[-A^T_{i-\frac{1}{2},2}\left(\psi_{i,2} - \psi_{i-1,2}\right) - A^T_{i+\frac{1}{2},2}\left(\psi_{i+1,2} - \psi_{i,2}\right)\right]$$
$$+\frac{1}{2}\left[-B^T_{i,\frac{5}{2}}\left(\psi_{i,3} - \psi_{i,2}\right)\right] + \Phi$$

$$(28)$$

where V is the cell area, Φ is the source term for inverse design,

$$\Phi = \left(-\Delta y_\xi\psi_{2_{i,2}} + \Delta x_\xi\psi_{3_{i,2}} - (p - p_T)\Delta s_i\right)\delta p_{i,2}$$

and,

$$A^T_{i+\frac{1}{2},2} = \Delta y_{\eta_{i+\frac{1}{2},2}}\left[\frac{\partial f}{\partial w}\right]^T_{i,2} - \Delta x_{\eta_{i+\frac{1}{2},2}}\left[\frac{\partial g}{\partial w}\right]^T_{i,2}$$

All the terms in equation (28) except for the source term are scaled as the square of Δx. Therefore, as the mesh width is reduced, the terms within parenthesis in the source term divided by Δs_i must approach zero as the solution reaches a steady state. One then recovers the continuous adjoint boundary condition as stated in equation (20).

If a first order artificial dissipation equation is used, then equation (27) would reduce to the term associated with ϵ^2. In such a case, the discrete adjoint equations are completely independent of the

costate variables in the cells below the wall. However, if we use the blended first and third order equation, then these values are required. As shown later, a simple zeroth order extrapolation across the wall produces good results.

Replacing the inverse design boundary condition in equation (28) by the discrete form of equation (24) results in a discrete adjoint equation for drag minimization.

Optimization Procedure

The search procedure used in this work is a simple descent method in which small steps are taken in the negative gradient direction. Let $\mathcal{F}$ represent the design variable, and $\mathcal{G}$ the gradient. Then an improvement can be made with a shape change

$$\delta\mathcal{F} = -\lambda\mathcal{G},$$

The gradient $\mathcal{G}$ can be replaced by a smoothed value $\overline{\mathcal{G}}$ in the descent process. This ensures that each new shape in the optimization sequence remains smooth and acts as a preconditioner which allows the use of much larger steps. To apply smoothing in the ξ_1 direction, the smoothed gradient $\overline{\mathcal{G}}$ may be calculated from a discrete approximation to

$$\overline{\mathcal{G}} - \frac{\partial}{\partial\xi_1}\epsilon\frac{\partial}{\partial\xi_1}\overline{\mathcal{G}} = \mathcal{G}$$

where ϵ is the smoothing parameter. If the modification is applied on the surface $\xi_2 = $ constant, then the first order change in the cost function is

$$\delta I = -\int\int\mathcal{G}\delta\mathcal{F}d\xi_1$$
$$= -\lambda\int\int\left(\overline{\mathcal{G}} - \frac{\partial}{\partial\xi_1}\epsilon\frac{\partial}{\partial\xi_1}\overline{\mathcal{G}}\right)\overline{\mathcal{G}}d\xi_1$$
$$= -\lambda\int\int\left(\overline{\mathcal{G}}^2 + \epsilon\left(\frac{\partial\overline{\mathcal{G}}}{\partial\xi_1}\right)^2\right)d\xi_1$$
$$< 0,$$

assuring an improvement if λ is sufficiently small and positive. The smoothing leads to a large reduction in the number of design iterations needed for convergence. An assessment of alternative search methods for a model problem is given by Jameson and Vassberg.[23]

7

Results

This section presents the results of the inviscid inverse design and drag minimization cases. For each case, we compare the continuous and discrete gradients, study the adjoint solutions from each method, and compare the convergence of the methods.

Inverse Design

The target pressure is first obtained using the FLO83 flow solver for the NACA 64A410 airfoil at a flight condition of $M = 0.74$ and a lift coefficient of $C_l = 0.63$ on a 192 x 32 C-grid. At such a condition the NACA 64A410 produces a strong shock on the upper surface of the airfoil, thus making it an ideal test case for the adjoint versus finite difference comparison.

The gradient for the continuous and discrete adjoint is obtained by perturbing each point on the airfoil. We apply an implicit smoothing technique to the gradient, before it is used to obtain a direction of descent for each point on the surface of the airfoil. Figure (1) illustrates an inverse design case of a Korn to NACA 64A410 airfoil at fixed lift coefficient. Figure (1a) shows the solution for the Korn airfoil at $M = 0.74$ and $C_l = 0.63$. After five design cycles we achieve a general shape of the target airfoil as shown in figure (1b). After twenty five design cycles the upper surface shape is obtained, and nearly eighty percent of the lower surface is achieved. Following a few more iterations, we obtain the desired target pressure except for a few points at the trailing edge. Observe the point-to-point match-up at the shock.

Figures (2), (3), and (4) exhibit the values of the gradients obtained from the adjoint methods and finite difference for various grid sizes. The circles denote values that we obtain by using the finite difference method. The square represents the discrete adjoint gradient. The asterisk represents the continuous adjoint gradient. The gradient is obtained with respect to variations in Hicks-Henne sine "bump" functions placed along the upper and lower surface of the airfoil.[3, 21] The figures only illustrate the values obtained from the upper surface starting from the leading edge on the left and ending at the trailing edge on the right. In order to reach an accurate finite difference gradient, we obtain gradients for various step sizes until the finite difference gradient for each point converges. The discrete adjoint equation is obtained from the discrete flow equations but without taking into account the dependence of the dissipa-

Grid Size	Cont.	Disc.	Cont-Disc
96 x 16	$3.106e-3$	$2.397e-3$	$9.585e-4$
192 x 32	$1.730e-3$	$1.724e-3$	$2.130e-4$
256 x 64	$1.424e-3$	$1.419e-3$	$4.749e-5$

Table 1: L_2 norm of the Difference Between Adjoint and Finite Difference Gradient

tion coefficients on the flow variables. Therefore, in order to eliminate the effect of this on comparisons with the finite difference gradient we compute the flow solution until attaining a decrease of seven orders of magnitude in the residue. We then freeze the dissipative coefficients and calculate the finite difference value for each design point. The figures show that the only discrepancies exist in the trailing edge area.

Table 1 contains values of the L_2 norm of the difference between the adjoint and finite difference gradients. The table illustrates three important facts: the difference between the continuous adjoint and finite difference gradient is slightly greater than that between the discrete adjoint and finite difference gradient; the norm decreases as the mesh size is increased; and the difference between continuous and discrete adjoint gradients decreases as the mesh size is reduced. The second column depicts the difference between the continuous adjoint and finite difference gradient. The third column depicts the difference between the discrete adjoint and finite difference gradients. The last column depicts the difference between the discrete adjoint and continuous adjoint. As the mesh size increases the norms decrease as expected. Since we derive the discrete adjoint by taking a variation of the discrete flow equations, we expect it to be consistent with the finite difference gradients and thus to be closer than the continuous adjoint to the finite difference gradient. This is confirmed by numerical results, but the difference is very small. As the mesh size increases, the difference between the continuous and discrete gradients should decrease, and this is reflected in the last column of table 1.

Figure (5) presents the effect of the partial discretization of the flow solver to obtain the discrete adjoint equation. Here we obtain the finite difference gradients in the figure without freezing the dissipative coefficients. A small discrepancy exists in regions closer to the leading edge and around the shock.

Kim, Alonso, and Jameson[21] verified that accurate finite difference gradients require a convergence

of four to five orders of magnitude in the flow solver. However, both the continuous and discrete adjoint gradients only require a convergence of two orders of magnitude in the flow solver. Figures (6) and (7) illustrate the continuous and discrete gradients for various flow solver convergence. In figure (8) and (9) continuous and discrete adjoint gradients are plotted for various adjoint solver convergence. The gradients only require two orders of magnitude convergence in the adjoint solver.

Figure (10) shows a comparison of the profiles of the second and third costate values between the continuous and discrete adjoint method in a direction normal to the boundary. The solutions agree in the interior points, differing only at the cell below the boundary due to the different treatment of the boundary condition. In the continuous case the value at cell one is updated by the boundary condition. This is in contrasts to the discrete case where the boundary condition appears as a source term when the fluxes are accumulated in cell two and the boundary condition does not depend on the value of the costate in cell one. In figure (11) both methods produce similar convergence histories.

In figure (12) we attempt to design a Korn airfoil based on the target pressure of the NACA 64A410 at a Mach number of 0.78. Both the initial and target pressures contain a very strong shock. A comparison of the finite difference and adjoint gradients reveals an increase in the discrepancy between the two gradients in the vicinity of the shock. In contrast to figure (2), where the shock location is at mesh point 75 along the surface, figure (13) illustrates the discrepancy around the stronger shock around mesh point 80.

Drag Minimization

The cost function for drag minimization is the pressure drag of the airfoil. We perform computations on a NACA 64A410 airfoil at a flight condition of $M = 0.75$ and fixed lift coefficient of $C_l = 0.63$. As before, the gradients were obtained by taking variations respect to Hicks-Henne sine "bump" functions placed along the upper and lower surface of the airfoil. Figure (15a) illustrates the initial solution of the airfoil with 132 drag counts. After two design cycles, the drag is reduced by a third to 44 drag counts. The strong shock in the initial solution is weakened. And after just four design cycles, this value is further halved. In figure (15d), the final design does not contain any shock and the drag count is a mere 15.

Grid Size	Cont.	Disc.	Cont-Disc
96 x 16	$2.920e-2$	$1.275e-2$	$2.009e-2$
192 x 32	$1.049e-2$	$7.577e-3$	$5.072e-3$
256 x 64	$6.241e-3$	$5.542e-3$	$1.315e-3$

Table 2: L_2 norm of the Difference Between Adjoint and Finite Difference Gradient

Figures (16-18) illustrate the values of the gradients obtained from the adjoint methods and finite difference for various grid sizes. The finite difference gradients are based on the same method used for the inverse design case, where the dissipative coefficients are frozen after a converged flow solution is obtained to simulate a full discretization for the discrete adjoint equation. We reduce the finite difference step sizes until we gain converged values for each design point. We plot gradients for the upper surface from leading edge to trailing edge. In figure (16) design points between 50 and 60 are located in the vicinity of the leading edge, where the gradient has a positive slope. In this region the discrete adjoint gradient agrees better with the finite difference gradient, if compared to the continuous adjoint gradient. The difference reduces as the grid size increases. Apart from the region of the leading edge, the adjoint and finite difference gradients agree.

Table (2) contains values of the L_2 norm of the difference between the adjoint and finite difference gradients. Similar to the inverse design case, the table illustrates three important facts: the discrete adjoint gradient is closer than the continuous adjoint gradient to the finite difference gradient; the norms decrease as the mesh size increases; and, finally, the difference between the continuous and discrete adjoint gradient decreases as the mesh size increases.

We recalculate the finite difference and adjoint gradients in figure (19) for the medium size mesh of 192 x 32 cells to illustrate the effect of partial discretization of the flow solver. The dissipative coefficients are not frozen during the finite difference calculations. A very small discrepancy appears in the leading edge and in the shock wave (points: 137-140).

Figures (20) and (21) illustrate the continuous and discrete gradients for various flow solver convergence. Only a single order magnitude drop in the flow solver is required for the adjoint gradients to converge. We plot continuous and discrete adjoint gradients in figure (22) and (23) for various adjoint solver convergence. The gradients only require one order of magnitude convergence in the adjoint solver.

Figure (24) shows a comparison of convergence of the objective function between the continuous and discrete adjoint. Both methods converge to the same value for the objective function. Figure (25) presents the second and third costate profiles normal to the boundary for the continuous and discrete adjoint solutions. Both solutions agree in the interior points but disagree at the cell below the wall. This is due to the difference between the enforcement of the boundary condition. Figure (26) shows that both adjoint methods produce the same convergence history.

Conclusion

This paper presents a complete formulation for the continuous and discrete adjoint approach to automatic aerodynamic design using the Euler equations. The gradients from each method are compared to finite difference gradients. We conclude:

1. The continuous boundary condition appears as an update to the costate values below the wall for a cell-centered scheme, and the discrete boundary condition appears as a source term in the cell above the wall. As the mesh width is reduced, one recovers the continuous adjoint boundary condition from the discrete adjoint boundary condition. (Equations 23 and 28)

2. Discrete adjoint gradients have better agreement than continuous adjoint gradients with finite difference gradients as expected, but the difference is generally small. (Figure 16)

3. As the mesh size increases, both the continuous adjoint gradient and the discrete adjoint gradient approach the finite difference gradient. (Figures 16-18)

4. The difference between the continuous and discrete gradient reduces as the mesh size increases. (Tables 1 and 2)

5. The cost of deriving the discrete adjoint is greater. (Equation 26)

6. With our search procedure as outlined, the overall convergence of the objective function is not significantly affected when the discrete adjoint gradient is used instead of the continuous adjoint gradient. Consequently, we find no particular benefit in using the discrete adjoint method, which requires greater computational cost. However, we believe it beneficial to use the discrete adjoint equation as a guide for the discretization of the continuous adjoint equation. (Figure 24)

Acknowledgments

References

[1] F. Bauer, P. Garabedian, D. Korn, and A. Jameson *Supercritical Wing Sections II.* Springer-Verlag, New York, 1975

[2] P. Garabedian, and D. Korn Numerical Design of Transonic Airfoils *Proceedings of SYNSPADE 1970.* pp 253-271, Academic Press, New York, 1971.

[3] R. M. Hicks and P. A. Henne. Wing Design by Numerical Optimization. *Journal of Aircraft.* 15:407-412, 1978.

[4] J.L. Lions. *Optimal Control of Systems Governed by Partial Differential Equations.* Springer-Verlag, New York, 1971. Translated by S.K. Mitter.

[5] O. Pironneau. *Optimal Shape Design for Elliptic Systems.* Springer-Verlag, New York, 1984.

[6] A. Jameson. Aerodynamic design via control theory. In *Journal of Scientific Computing,* 3:233-260,1988.

[7] A. Jameson. Automatic design of transonic airfoils to reduce the shock induced pressure drag. In *Proceedings of the 31st Israel Annual Conference on Aviation and Aeronautics, Tel Aviv,* pages 5–17, February 1990.

[8] A. Jameson. Optimum aerodynamic design using CFD and control theory. *AIAA paper 95-1729,* AIAA 12th Computational Fluid Dynamics Conference, San Diego, CA, June 1995.

[9] A. Jameson., N. Pierce, and L. Martinelli. Optimum aerodynamic design using the Navier-Stokes equations. In *AIAA 97-0101,* 35th. Aerospace Sciences Meeting and Exhibit, Reno, Nevada, January 1997.

American Institute of Aeronautics and Astronautics

[10] A. Jameson., L. Martinelli, and N. Pierce Optimum aerodynamic design using the Navier-Stokes equations. In *Theoretical Computational Fluid Dynamics*, 10:213-237, 1998.

[11] G. R. Shubin and P. D. Frank A Comparison of the Implicit Gradient Approach and the Variational Approach to Aerodynamic Design Optimization. *Boeing Computer Services Report AMS-TR-163*, April 1991.

[12] J. Reuther and A. Jameson. Aerodynamic shape optimization of wing and wing-body configurations using control theory. *AIAA 95-0213*, 33rd Aerospace Sciences Meeting and Exibit, Reno, Nevada, January 1995.

[13] J. Reuther, A. Jameson, J. Farmer, L. Martinelli, and D. Saunders. Aerodynamic shape optimization of complex aircraft configurations via an adjoint formulation. *AIAA 96-0094*, AIAA 34th Aerospace Sciences Meeting and Exhibit, Reno, NV, January 1996.

[14] J. Reuther, A. Jameson, J. J. Alonso, M. J Rimlinger, and D. Saunders. Constrained multipoint aerodynamic shape optimization using an adjoint formulation and parallel computers. *AIAA 97-0103*, AIAA 35th Aerospace Sciences Meeting and Exhibit, Reno, NV, January 1997.

[15] F. Beux and A. Dervieux. Exact-Gradient Shape Optimization of a 2-D Euler Flow. *Finite Elements in Analysis and Design*, Vol. 12, 1992, 281-302.

[16] G. W. Burgreen and O. Baysal. Three-Dimensional Aerodynamic Shape Optimization of Wings Using Discrete Sensitivity Analysis. *AIAA Journal*, Vol. 34, No.9, September 1996, pp. 1761-1770.

[17] J. Elliot and J. Peraire. Aerodynamic Design Using Unstructured Meshes. *AIAA 96-1941*, 1996.

[18] W. K. Anderson and V. Venkatakrishnan Aerodynamic Design Optimization on Unstructured Grids with a Continuous Adjoint Formulation. *AIAA 96-1941*, 1996.

[19] A. Iollo, M. Salas, and S. Ta'asan. Shape Optimization Gorvened by the Euler Equations Using and Adjoint Method. *ICASE report 93-78*, November 1993.

[20] S. Ta'asan, G. Kuruvila, and M. D. Salas. Aerodynamic design and optimization in one shot. *AIAA 91-0025*, 30th Aerospace Sciences Meeting and Exibit, Reno, Nevada, January 1992.

[21] S. Kim,J. J. Alonso, and A. Jameson A Gradient Accuracy Study for the Adjoint-Based Navier-Stokes Design Method. *AIAA 99-0299*, AIAA 37th. Aerospace Sciences Meeting and Exhibit, Reno, NV, January 1999.

[22] A. Jameson Solution of the Euler Equations for Two Dimensional Transonic Flow By a Multigrid Method. *Applied Mathematics and Computation*, 13:327-355, 1983.

[23] A. Jameson Studies of Alternative Numerical Optimization Methods Applied to the Brachistochrone Problem.

11
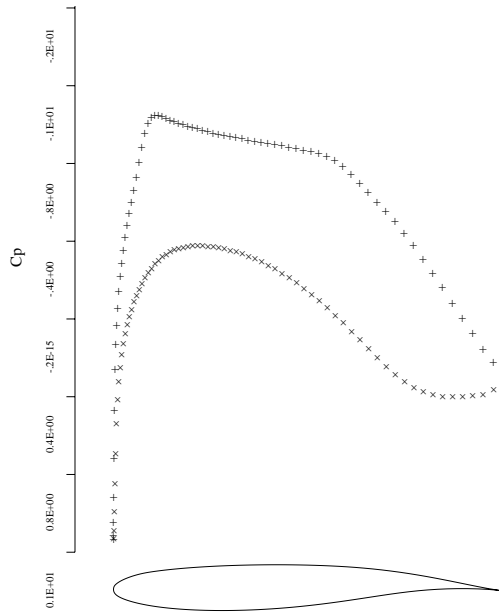
1a: Initial Solution of Korn Airfoil
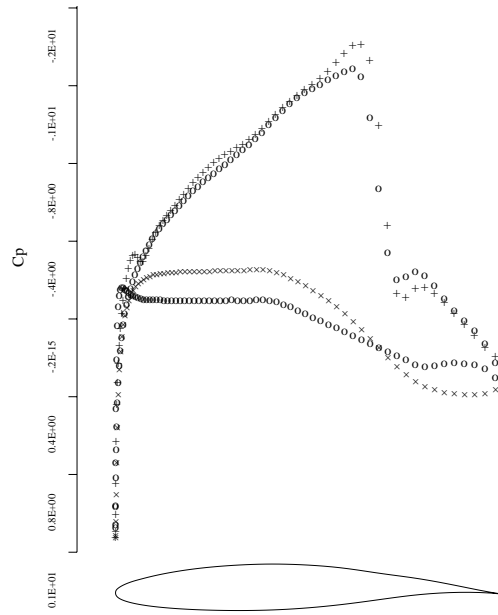
1b: After 5 Design Iterations
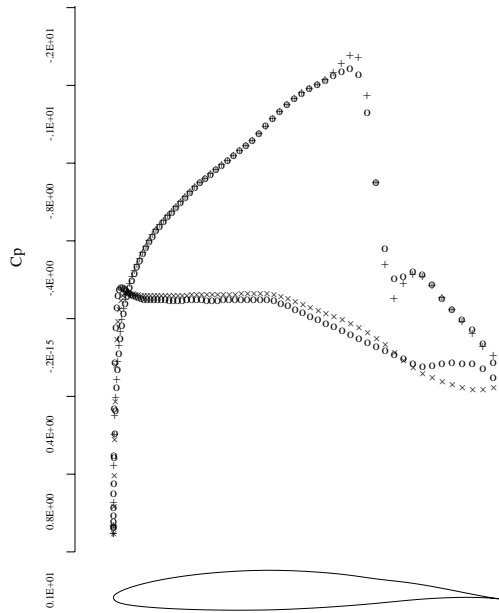
1c: After 25 Design Iterations
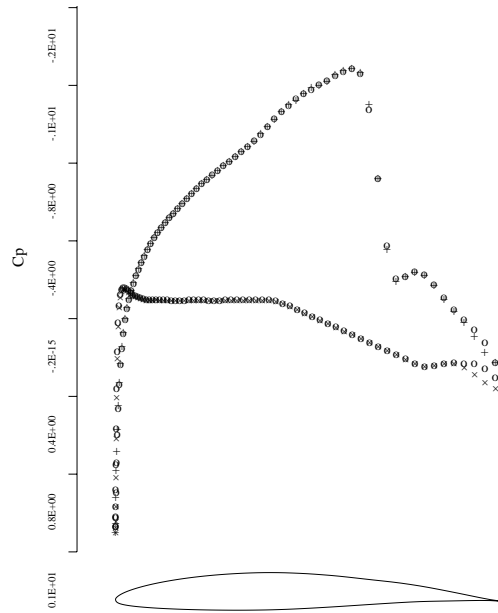
1d: Final Design

Figure 1: Inverse Design of Korn to NACA 64A410 at Fixed C_l
Grid - 192 x 32, $M = 0.74$, $C_l = 0.63$, $\alpha = 0$ degrees
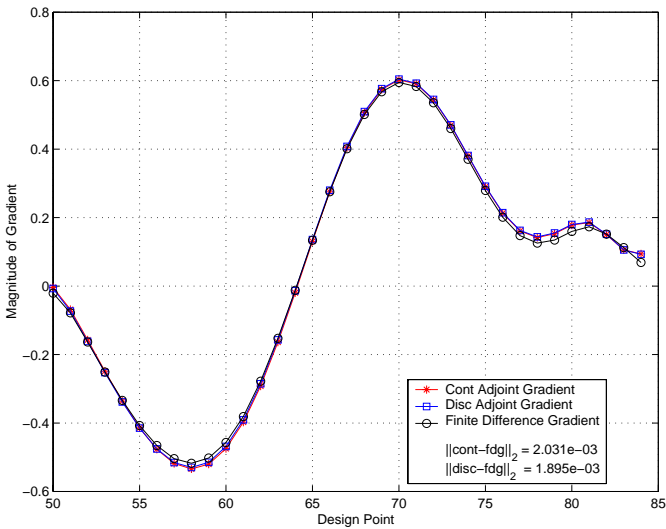
12

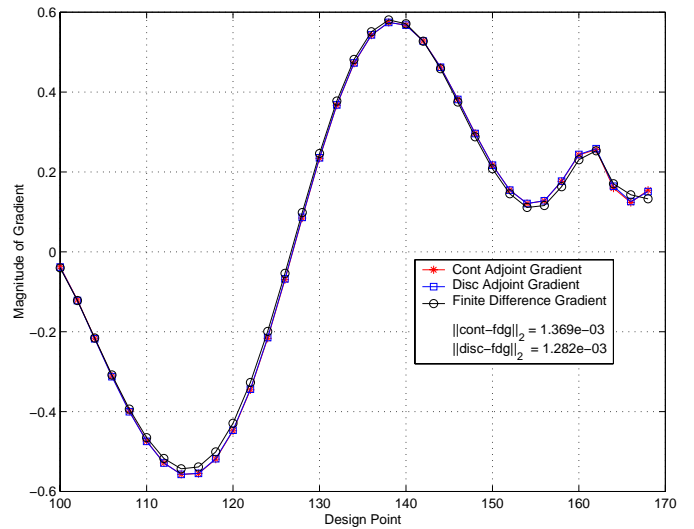American Institute of Aeronautics and Astronautics
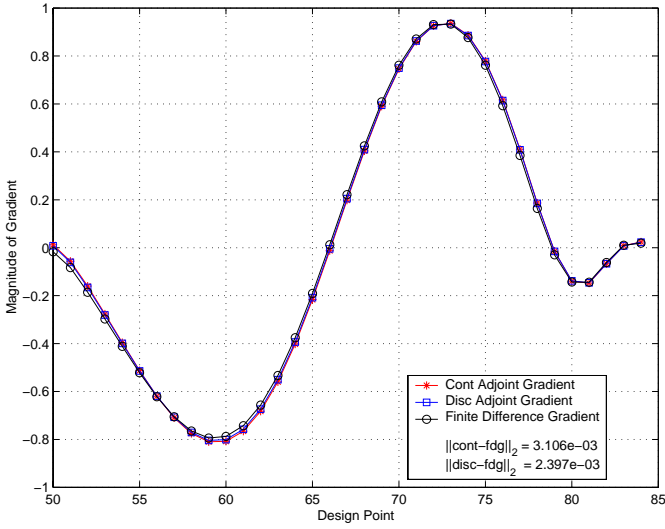
Figure 2: Adjoint Versus Finite Difference Gradients for Inverse Design of Korn to NACA 64A410 at Fixed C_l.
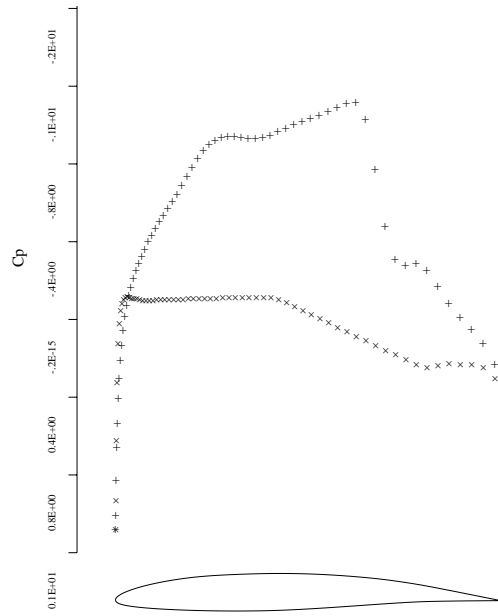Coarse Grid - 96 x 16, $M = 0.74$, $C_l = 0.63$
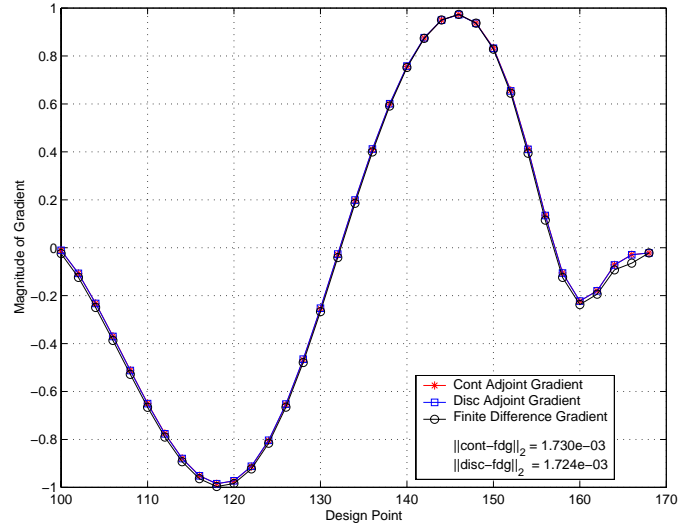
Figure 3: Adjoint Versus Finite Difference Gradients for Inverse Design of Korn to NACA 64A410 at Fixed C_l.
Medium Grid - 192 x 32, $M = 0.74$, $C_l = 0.63$
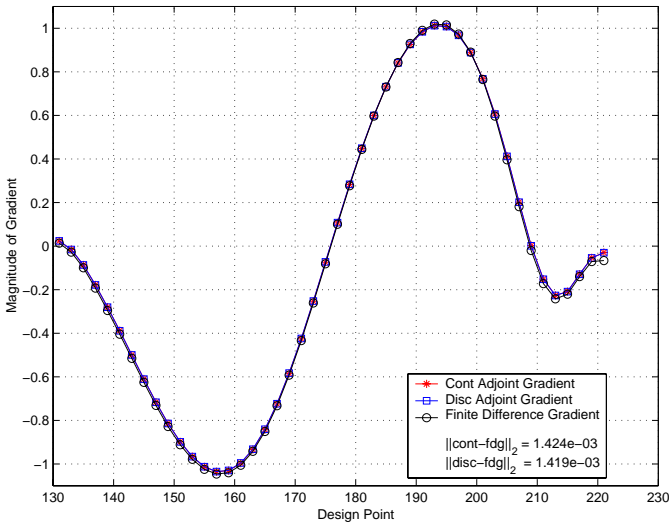
Figure 4: Adjoint Versus Finite Difference Gradients for Inverse Design of Korn to NACA 64A410 at Fixed C_l.
Fine Grid - 256 x 64, $M = 0.74$, $C_l = 0.63$
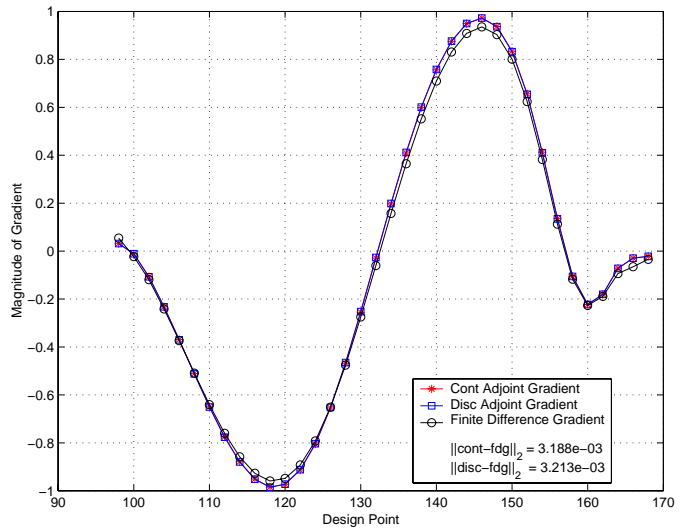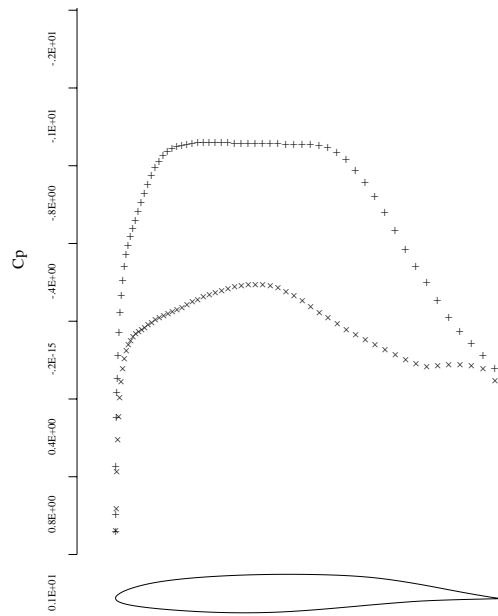

Figure 5: Adjoint Versus Finite Difference Gradients for Inverse Design of Korn to NACA 64A410 at Fixed C_l. Dissipative Coefficients Not Frozen
Medium Grid - 192 x 32, $M = 0.74$, $C_l = 0.63$

13
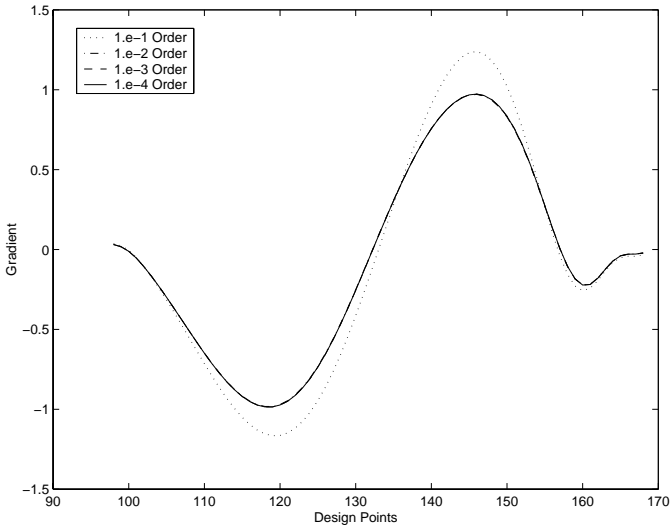
Figure 6: Continuous Adjoint Gradients for Varying Flow Solver Convergence for the Inverse Design Case
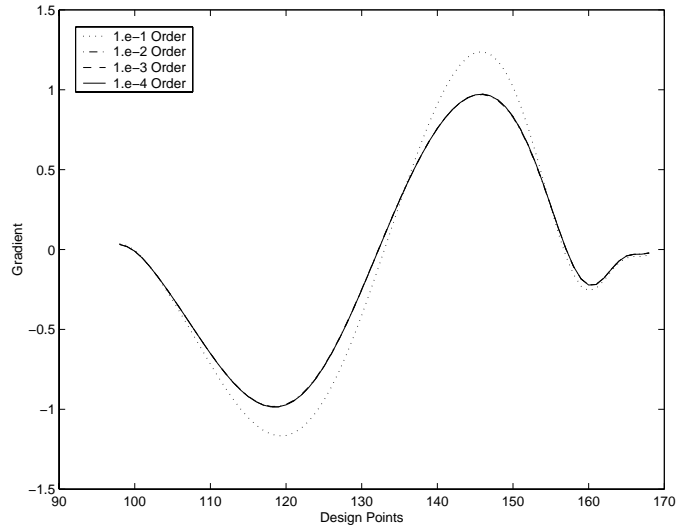
Figure 7: Discrete Adjoint Gradients for Varying Flow Solver Convergence for the Inverse Design Case
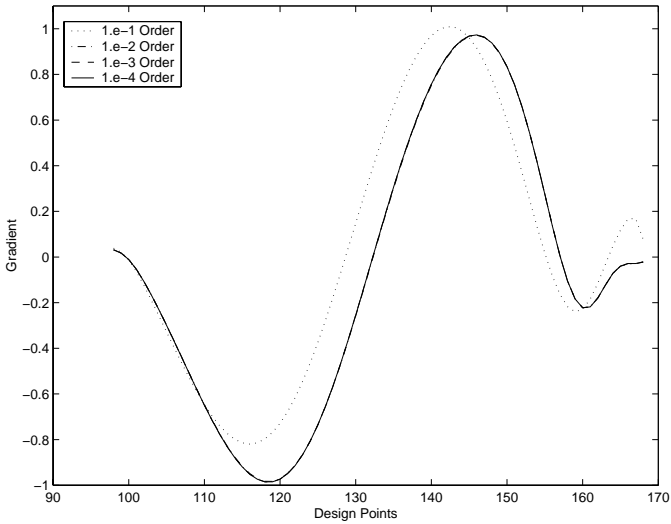
Figure 8: Continuous Adjoint Gradients for Varying Adjoint Solver Convergence for the Inverse Design Case
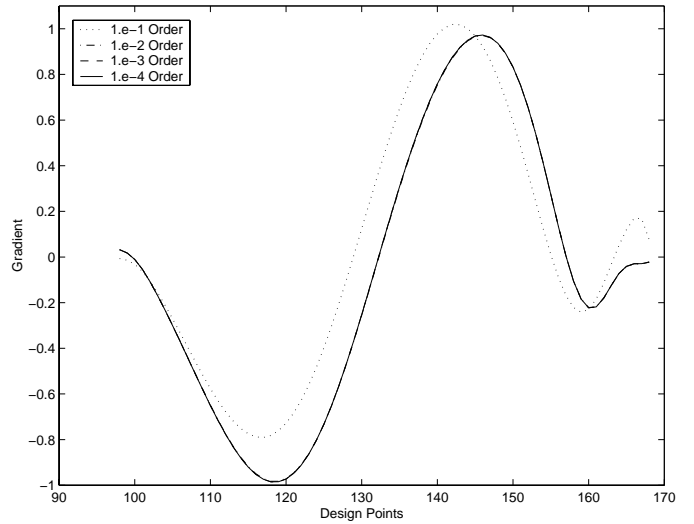
Figure 9: Discrete Adjoint Gradients for Varying Adjoint Solver Convergence for the Inverse Design Case

14
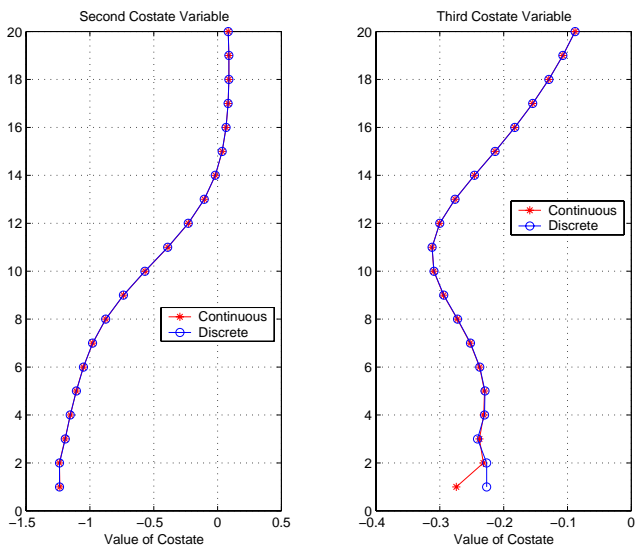
Figure 10: Comparison of Costate Values Between the Continuous and Discrete Adjoint Method for the Inverse Design of Korn to NACA 64A410 at Fixed C_l. Medium Grid - 192 x 32, $M = 0.74$, $C_l = 0.63$
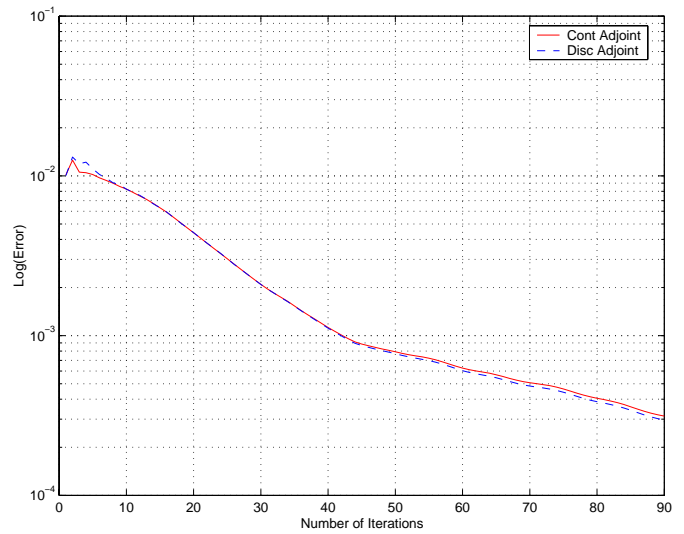
Figure 11: Convergence History for the Continuous and Discrete Adjoint for the Inverse Design of Korn to NACA 64A410 at Fixed C_l. $M = 0.74$, $C_l = 0.63$

American Institute of Aeronautics and Astronautics
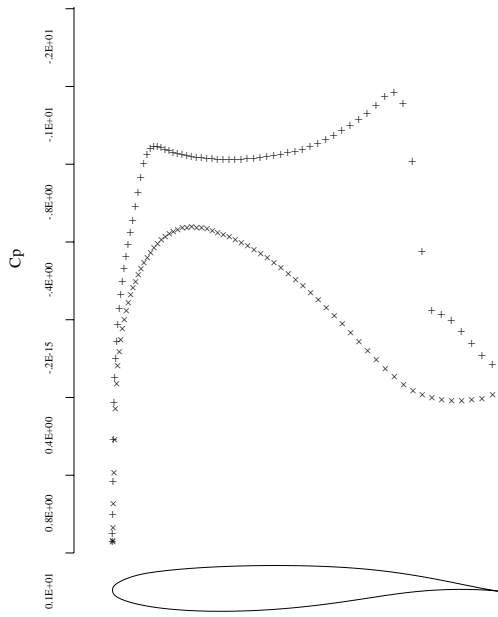
12a: Initial Solution of Korn Airfoil
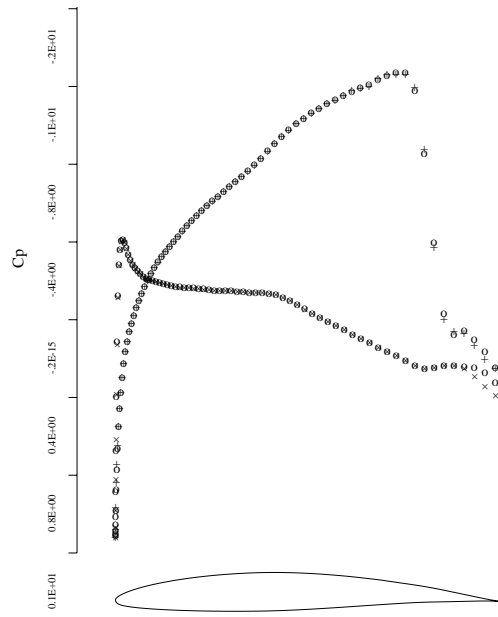
12b: Final Design

Figure 12: Inverse Design of Korn to NACA 64A410 at Fixed C_l
Grid - 192 x 32, $M = 0.78$, $C_l = 0.63$, $\alpha = 0$ degrees

Figure 13: Adjoint Versus Finite Difference Gradients for Inverse Design of Korn to NACA 64A410 at Fixed C_l.
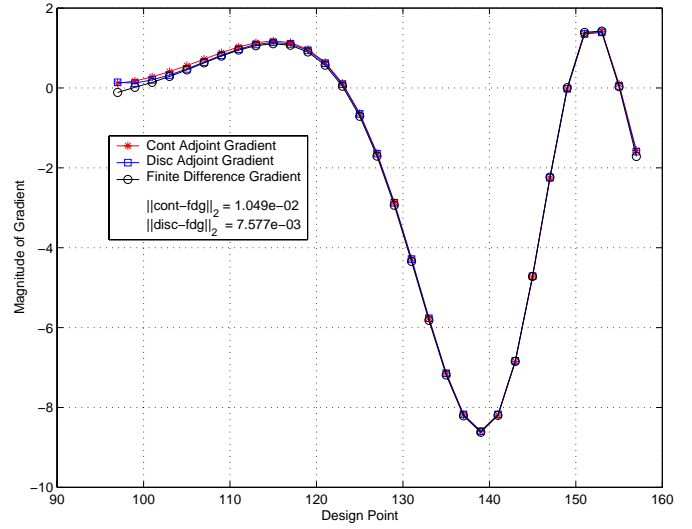Coarse Grid - 96 x 16, $M = 0.78$,
$C_l = 0.63$

Figure 14: Adjoint Versus Finite Difference Gradients for Inverse Design of Korn to NACA 64A410 at Fixed C_l.
Medium Grid - 192 x 32, $M = 0.78$,
$C_l = 0.63$

16
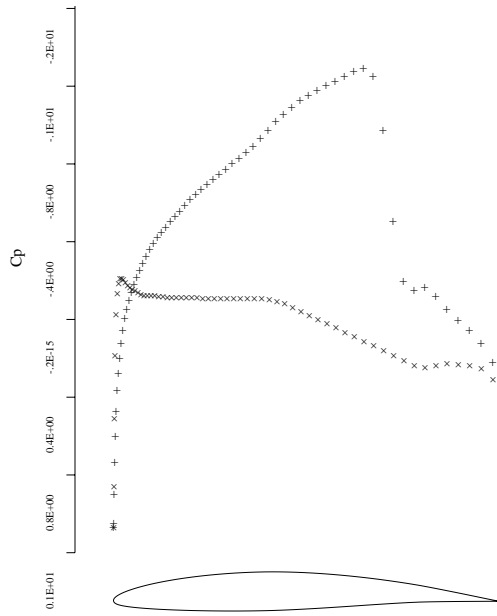
15a: Initial Solution of NACA 64A410.
$M = 0.75$, $C_l = 0.630$, $C_d = 0.0132$,
$\alpha = -.34$ degrees

15b: After 2 Design Iterations.
$M = 0.75$, $C_l = 0.626$, $C_d = 0.0044$,
$\alpha = -.18$ degrees
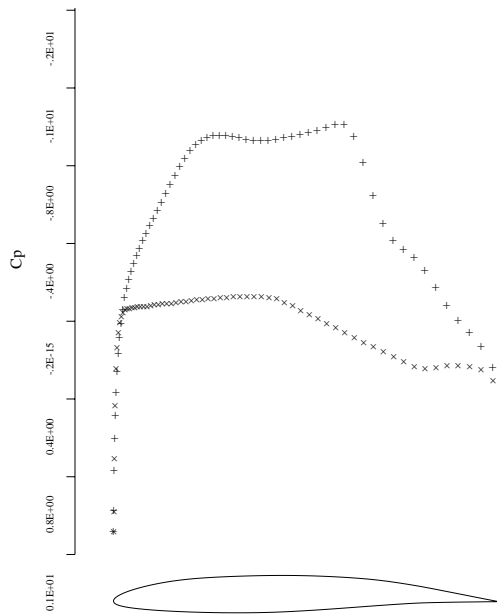
15c: After 4 Design Iterations
$M = 0.75$, $C_l = 0.626$, $C_d = 0.0022$,
$\alpha = -.08$ degrees

15d: After 20 Design Iterations
$M = 0.75$, $C_l = 0.629$, $C_d = 0.0015$,
$\alpha = .79$ degrees

Figure 15: Drag Minimization of NACA 64A410 at Fixed C_l
Grid - 192 x 32, $M = 0.75$, $C_l = 0.63$

17
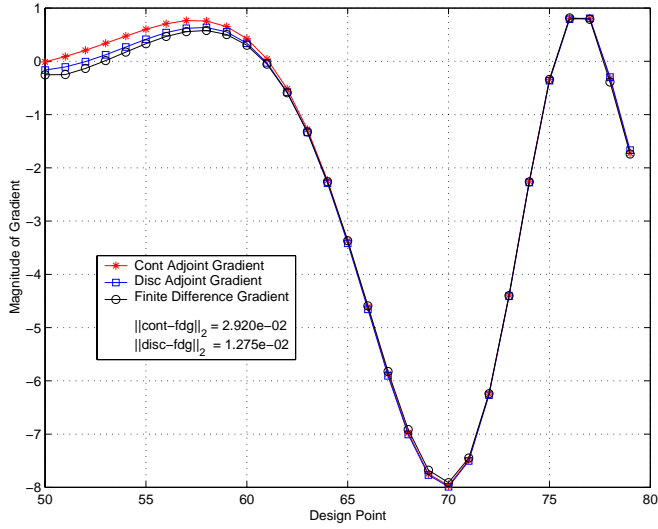
Figure 16: Adjoint Versus Finite Difference Gradients for Drag Minimization of NACA 64A410 at Fixed C_l.
Coarse Grid - 96 x 16, $M = 0.75$,
$C_l = 0.63$

Figure 17: Adjoint Versus Finite Difference Gradients for Drag Minimization of NACA 64A410 at Fixed C_l.
Medium Grid - 192 x 32, $M = 0.75$,
$C_l = 0.63$
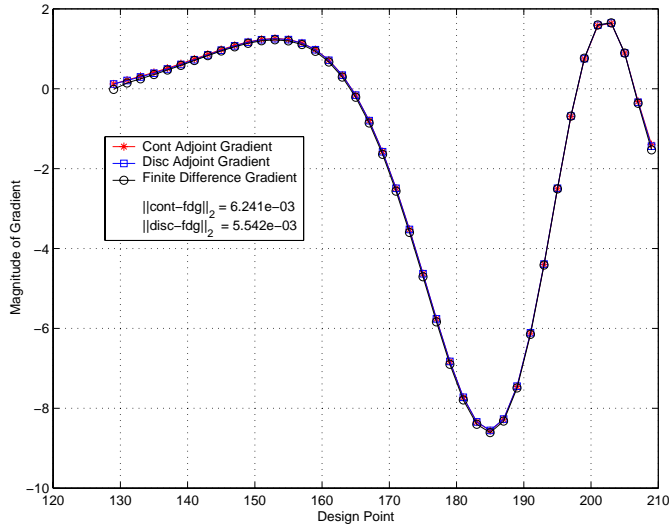
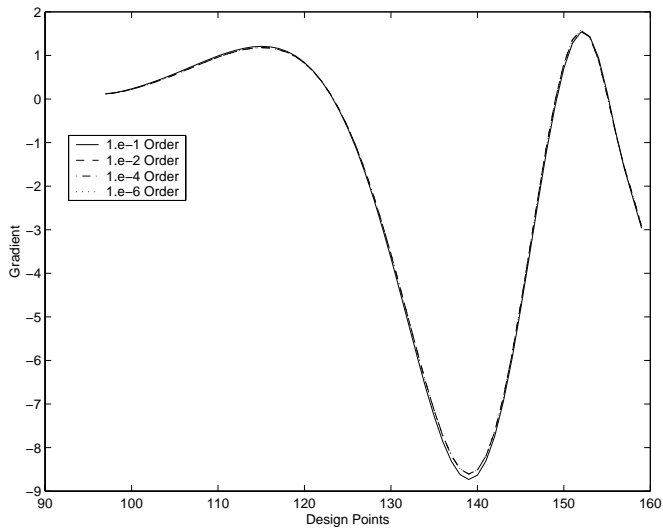Figure 18: Adjoint Versus Finite Difference Gradients for Drag Minimization of NACA 64A410 at Fixed C_l.
Fine Grid - 256 x 64, $M = 0.75$,
$C_l = 0.63$
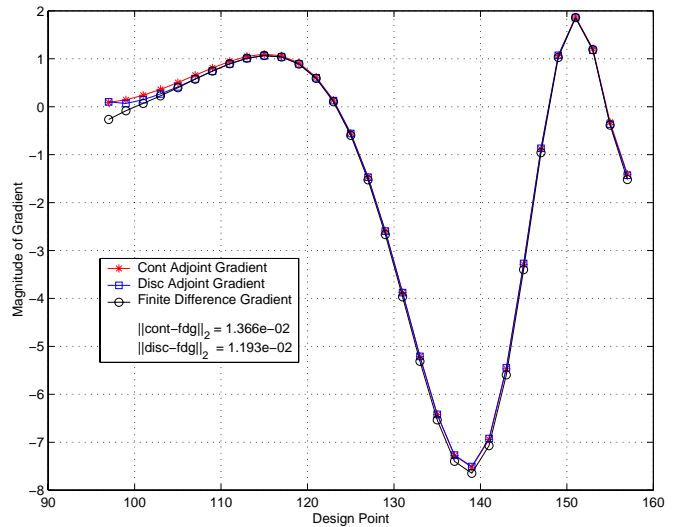
Figure 19: Adjoint Versus Finite Difference Gradients for Drag Minimization of NACA 64A410 at Fixed C_l. Dissipative Coefficients Not Frozen
Medium Grid - 192 x 32, $M = 0.75$,
$C_l = 0.63$

American Institute of Aeronautics and Astronautics

Figure 20: Continuous Adjoint Gradients for Varying Flow Solver Convergence for the Drag Minimization Case
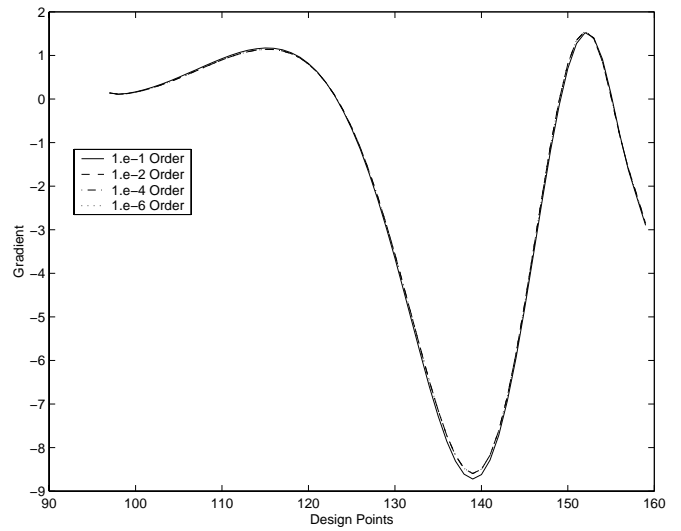
Figure 21: Discrete Adjoint Gradients for Varying Flow Solver Convergence for the Drag Minimization Case
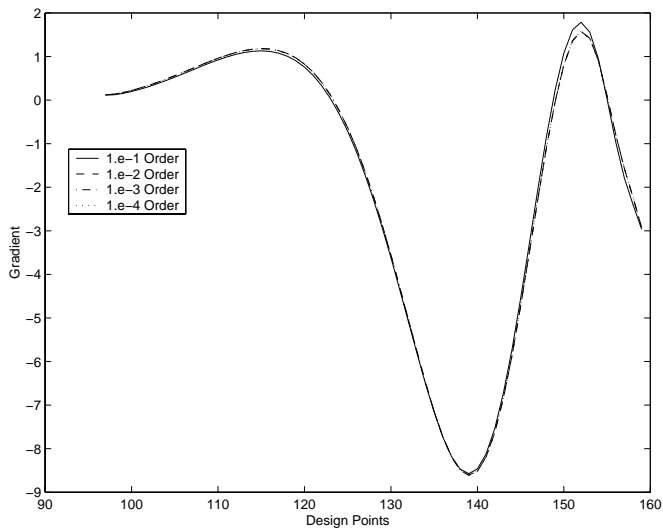

Figure 22: Continuous Adjoint Gradients for Varying Adjoint Solver Convergence for the Drag Minimization Case
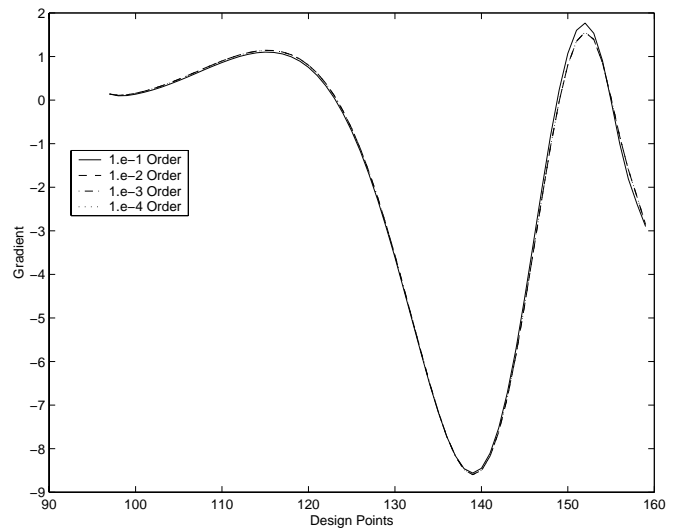

Figure 23: Discrete Adjoint Gradients for Varying Adjoint Solver Convergence for the Drag Minimization Case
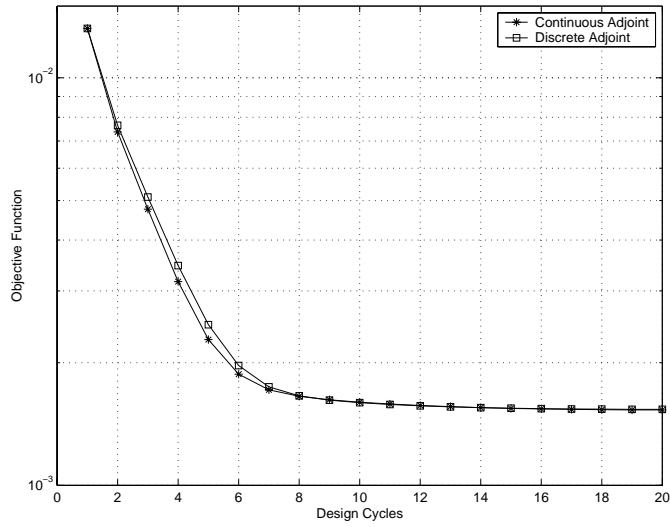
19

Figure 24: Comparison of Convergence of the Objective Function Between the Continuous and Discrete Adjoint Method for Drag Minimization
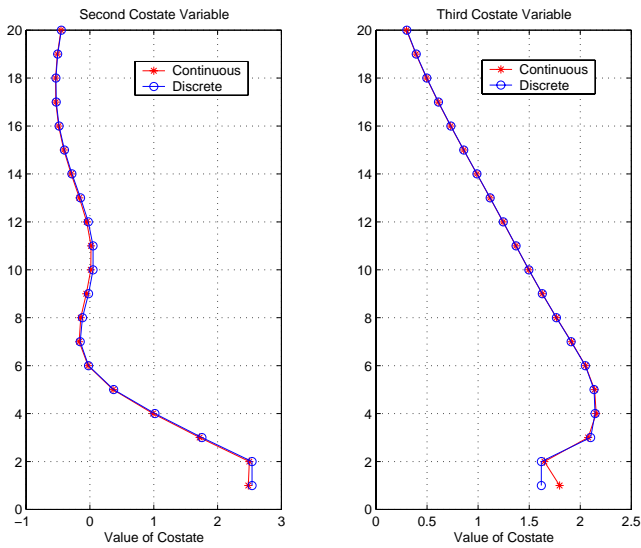

Figure 25: Comparison of Costate Values Between the Continuous and Discrete Adjoint Method for Drag Minimization of NACA 64A410 at Fixed C_l.
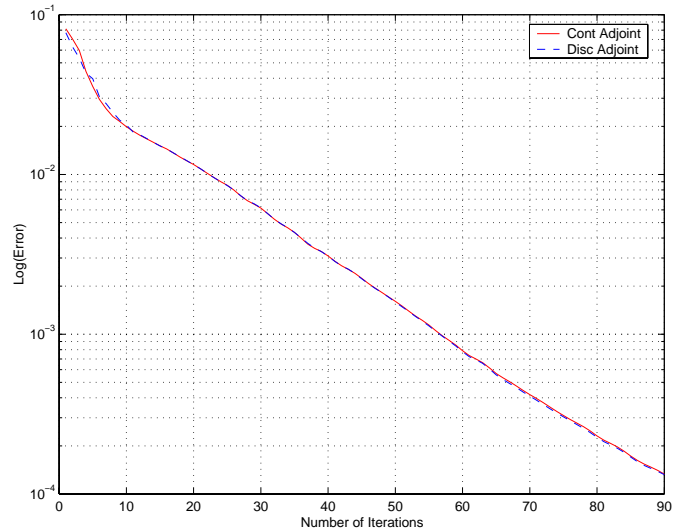Medium Grid - 192 x 32, $M = 0.75$, $C_l = 0.63$

Figure 26: Convergence History for the Continuous and Discrete Adjoint for Drag Minimization of NACA 64A410 at Fixed C_l. $M = 0.75$, $C_l = 0.63$

American Institute of Aeronautics and Astronautics